Lentivirus-mediated microRNA-26a overexpression in bone mesenchymal stem cells facilitates bone regeneration in bone defects of calvaria in mice

ZHI LIU[1,2], HONG CHANG[1], YIHONG HOU[1], YU WANG[1], ZHIQIANG ZHOU[2], MING WANG[2], ZHIDONG HUANG[2] and BIN YU[1]

[1]Department of Orthopedics and Traumatology, Nanfang Hospital, Southern Medical University, Guangzhou, Guangdong 510515; [2]Department of Surgery II, People's Hospital of Dongsheng, Ordos City, Inner Mongolia 017000, P.R. China

Received July 14, 2017; Accepted March 1, 2018

DOI: 10.3892/mmr.2018.9596

Abstract. Repair of bone defects presents a serious clinical challenge as it is difficult to restore bone function and regenerate bone loss. In the present study, the effects of lentivirus-mediated transfection of bone marrow mesenchymal stem cells (BMSCs) with microRNA (miR)-26a on bone regeneration were investigated in a mouse bone defect repair model. Marker of proliferation Ki67 (Ki67) staining was employed to detect the cell proliferation capacity and alkaline phosphatase (ALP) staining was used to investigate osteogenic differentiation. A mouse model of cranial bone defects was established. β-tricalcium phosphate biomaterials co-cultured with the transfected BMSCs were implanted into the defect areas of mouse models. Micro-computed tomography, and hematoxylin and eosin and toluidine blue staining, were used to detect bone regeneration in the defect areas and the degradation of scaffolds. miR-26a expression, and the mRNA and protein expression of osteogenesis-associated cytokines, were detected using reverse transcription-quantitative polymerase chain reaction and western blot analysis. Separated and cultured BMSCs highly expressed CD29 and CD105, but not CD34 and CD45, as determined by flow cytometry. miR-26a expression and the positive cell rate of Ki67 and ALP staining in BMSCs transfected with pLVTHM-miR-26a were increased. The BMSC and negative control-transfected BMSC groups exhibited increased bone regeneration in the defect areas, increased bone volume of newly formed bones, and elevated mRNA and protein expression of runt-related transcription factor 2 (Runx2) and osteocalcin (OC), compared with the blank group. However, the miR-26a-transfected BMSC group exhibited further increases in bone regeneration and the volume of newly formed bones, and further elevations of the mRNA and protein expression levels of Runx2 and OC. The present findings demonstrated that lentivirus-mediated modification of BMSCs enhanced bone regeneration during the repair of cranial bone defects in mice.

Correspondence to: Dr Bin Yu, Department of Orthopedics and Traumatology, Nanfang Hospital, Southern Medical University, 1838 North of Guangzhou Avenue, Guangzhou, Guangdong 510515, P.R. China
E-mail: yubinol1204@163.com

Key words: microRNA-26a, lentivirus-mediated, bone marrow mesenchymal stem cells, gene modification, bone defect, bone regeneration

Introduction

Bone defects are commonly caused by traumatic events, chronic infection or bone tumor resection, which pose critical clinical issues and rapidly increasing morbidity (1). The severity of bone defects is associated with the specific skeletal segment involved and the degree of bone loss, specifically 6 cm for the humerus, 5 cm for the femur and tibia, and 3 cm for the forearm (2). It has been noted that osteogenesis is a key factor in the process of bone formation (3,4). The gold standard for bone repair and healing is autologous and allogeneic bone grafting in patients with large bone defects or fracture non-unions (5). However, this treatment method is limited due to donor shortages, infectious diseases, nerve injury, persistent pain and potential new fractures (6). These limitations motivate additional investigations to develop improved techniques or treatment regimens for bone defects, and therapies based on bone marrow mesenchymal stem cells (BMSCs) may lead to the improved repair of bone defects (7,8). Seed cells are essential for the treatment of bone defects; therefore, genetically modified BMSCs are widely employed in tissue engineering to improve osteogenesis and angiogenesis in bone regeneration (9). Multiple studies have documented the regulatory role of microRNAs (miRNAs/miRs) in the osteogenic differentiation of BMSCs, including miR-125b and miR-16 (10-12).

miRNAs refer to a group of conserved, short non-coding RNAs of 20-22 nucleotides that are closely associated with gene expression at post-transcriptional levels (13,14). Additionally, miRNAs modulate numerous cellular activities by binding to the 3'-untranslated region (3'-UTR) of their target

mRNAs (15,16). miRNAs are commonly aberrantly expressed in pathological alterations, and lentiviral vectors are frequently adopted to regulate the expression of miRNAs, which often serve as potential therapeutic targets (17,18). In terms of the osteogenesis of bone healing or repair, miRNAs have been demonstrated to be regulators, and miR-26a has already been demonstrated to be involved in osteogenic differentiation by targeting SMAD family member 1, as miR-26a is upregulated during osteoblast differentiation (19,20). Cytokines associated with osteogenesis, such as runt-related transcription factor 2 (Runx2) and osteocalcin (OC), are crucial osteogenic genes in bone regeneration of cranial bone defects (21). Accordingly, the present study investigated whether using BMSCs that overexpressed miR-26a, via lentivirus-mediated transfection, as seed cells may improve bone regeneration during the repair process of bone defects in a mouse model.

Materials and methods

Experimental animals and treatment. Male C57BL/6J mice aged 4 weeks (n=10; weight, 16.68±0.35 g; used for the cell separation) and 8 weeks (n=32; weight, 20.25±0.57 g; used for bone defect model experiments) were purchased from Shanghai SLAC Laboratory Animal Co., Ltd. (Shanghai, China). Mice were housed under a controlled temperature of 18-28˚C, a relative humidity of 40-70%, air cleanliness (100,000, ISO 8), background noise ≤60 dB and kept on a 12 h light/dark cycle. Free access to food and water and regular ventilation and disinfection were guaranteed for mice. Animal use and experimental procedures were performed in accordance with the Declaration of Helsinki (22) and the present study was approved by the Experimental Animal Ethics Committee of the People's Hospital of Dongsheng (Ordos City, China). The 32 male C57BL/6J 8-week-old mice were equally assigned to groups: Blank group (n=8, mice implanted with β-tricalcium phosphate (β-TCP) scaffolds alone in the defect area), BMSC group (n=8, mice implanted with β-TCP scaffolds co-cultured with BMSCs in the defect area), NC-BMSC group (n=8, mice implanted with β-TCP scaffolds co-cultured with negative control (NC)-transfected BMSCs in the defect area) and miR-26a-BMSC group (n=8, mice implanted with β-TCP scaffolds co-cultured with miR-26a-transfected BMSCs in the defect area).

BMSC isolation and culture. The thigh bones of both sides were separated from the male C57BL/6J mice (n=10; 4-weeks old) under sterile conditions. Following washing with PBS, the metaphyses of both sides were resected and attached muscles and fibrous tissues were also scraped off. A syringe pipette (1 ml) was used to pipette 5 ml α-minimum essential medium containing 10% fetal bovine serum (FBS; both Gibco; Thermo Fisher Scientific, Inc., Waltham, MA, USA), which was also supplemented with 100 U/ml penicillin and 100 U/ml streptomycin, to rinse the thigh bones. The mixture was triturated evenly to resuspend cells. Subsequently, cells were inoculated in culture flasks at a density of $1x10^6$ cells/ml and incubated in a 5% CO_2 incubator at 37˚C. The medium was renewed every three days. When adherent cells grew to 80-90% confluency, the culture medium was discarded. Following washing with PBS twice, cells were digested with 0.25% trypsin at room temperature and subcultured to a ratio of 1:3.

Flow cytometric analysis of BMSCs. Third generation BMSCs were digested with 0.25% trypsin and washed using PBS containing bovine serum albumin (BSA; 20%; Sigma-Aldrich; Merck KGaA, Darmstadt, Germany). The cells were subsequently resuspended in complete medium (Suzhou Cyagen Biosciences Inc., Suzhou, China) to a single cell suspension at a density of $5x10^6$ cells/ml. Eppendorf tubes were used to contain the single cell suspension and each tube was filled with 200 µl of the suspension ($5x10^6$ cells/ml). Rat anti-mouse antibodies against CD29 [fluorescein isothiocyanate (FITC)-conjugated; cat. no. 555005; 1:500), CD34 (FITC-conjugated; cat. no. 560238; 1:500), CD105 (phycoerythrin-conjugated; cat. no. 562759; 1:500) and CD45 (phycoerythrin-conjugated; cat. no. 553081; 1:500) and fluorescein isothiocyanate-labeled mouse IgG (cat. no. 555748; 1:500; all BD Biosciences, Franklin Lakes, NJ, USA) for flow cytometric detection were supplemented to the EP tubes, incubated at 4˚C for 60 min, washed with PBS containing 3% FBS 3 times and resuspended following centrifugation at 112 x g at 4˚C for 5 min and fixed with 200 µl polyoxymethylene (4%) at 4˚C for 1 h. A flow cytometer and Cell-Quest software (version 5.1; BD Biosciences) were used to analyze the cell phenotype.

Construction and determination of the lentiviral vector pLVTHM-miR-26a. The sequence of the miR-26a precursor pre-miR-26a-1 (accession no. MI0000083), with a full length of 77 bp, was obtained from the miRBase Sequence database (http://www.mirbase.org/), and flanking sequences (50 bp) were added both upstream and downstream of pre-miR-26a-1, which produced precursor fragments, including hairpin pre-miR-26a-1, which had a full length of 177 bp. The primer sequences were designed and synthesized by Shanghai Gene Pharma Co., Ltd. (Shanghai, China). Forward, 5'-CGACGC GTCGAGCCA AGAGCAGGAGGAC-3' and reverse, 5'-CCA TCGATGGTGGTGTTGGTGCCTCTGG-3'. Genomic DNA was extracted from the blood (65-100 µl) of 4 week old mice, obtained from retro-orbital blood using a heparinized micro-capillary tube. The blood was expelled immediately into a 1.5 ml microfuge tube containing 20 µl of 10 mM EDTA and mixed immediately to prevent clot formation. Then, 200 µl Lysis Buffer was added to each tube and agitated to suspend evenly. Centrifugation (16,000 x g at 4˚C for 25 sec) was used to pellet nuclei. The supernatant was removed and discarded and the above steps repeated 3 times. The nuclear pellet was resuspended in 100 µl PBND buffer (50 mM KCl; 10 mM Tris-HCl, pH 8.3; 2.5 mM $MgCl_2 \cdot 6H_2O$; 0.1 mg/ml gelatin; 0.45% v/v Nonidet P-40; 0.45% v/v Tween-20) with 60 µg/ml proteinase K and incubated overnight at 4˚C. Samples were heated to 97˚C for 10 min to inactivate proteinase K. Then, 1-5 µl of DNA solution was added for a 25 µl PCR reaction. Using the genomic DNA as a template, the primer sequences were amplified by polymerase chain reaction (PCR) to obtain fragments. The thermocycling conditions were: 98˚C for 3 min; 95˚C for 30 sec, 60˚C for 30 sec and 72˚C for 1.5 min, for 35 cycles. Following agarose gel electrophoresis, the amplified products and vector pLVTHM (held in our laboratory) were digested with *Mlu I* and *Cla I*, respectively. The

enzyme digestion products were incubated with ligase at 16˚C overnight and 20 μl transformed into 100 μl *Escherichia coli* DH-5α-competent cells (Transgen, Beijing, China), with empty vector (0.1 μg/μl) as a control. Positive recombinant clones were selected to conduct dual-enzyme (*Mlu I* and *Cla I*) digestion and were verified by PCR. Correct plasmids were verified via DNA sequencing by Shanghai GenePharma Co., Ltd. Lipofectamine® 2000 (Invitrogen; Thermo Fisher Scientific, Inc.) was used to transfect the successfully verified recombinant plasmids into 293T cells (>1x10^6/ml, Shanghai Genechem Co., Ltd., Shanghai, China) at the logarithmic growth phase. Following 72 h transfection, the supernatant of 293T cells was collected to prepare the virus suspension. Following this, resuspended 293T cells (>1x10^6/ml) were supplemented with the virus suspension and incubated at 37˚C for 24 h to measure the lentiviral titer.

Infection of BMSCs with the lentiviral vector pLVTHM-miR-26a. BMSCs of mice were inoculated in sterile petri dishes (6 cm). When cells grew to 30-45% confluency, supernatant of the lentiviral vector pLVTHM-miR-26a (8 μg/ml) and empty vector pLVTHM (8 μg/ml) were added. Reverse transcription-quantitative PCR (RT-qPCR) was applied to detect the expression levels of miR-26a 48 h later. BMSCs successfully infected with the lentiviral vector pLVTHM-miR-26a were termed the miR-26a-BMSC group. BMSCs infected with the empty vector pLVTHM were termed the NC-BMSC group.

MTT assay to detect cell viability. BMSCs were inoculated in a 96-well plate with 5x10^4 cells per well, and each group was repeated in six wells. When cells reached 80% confluency, they were grouped as follows: BMSC group, NC-BMSC group (BMSCs infected with the pLVTHM empty vector) and miR-26a-BMSC group (BMSCs infected with pLVTHM-miR-26a). MTT solution (20 μl; Sigma-Aldrich; Merck KGaA, Darmstadt, Germany) was added, followed by incubation at 37˚C in an incubator for 4 h. MTT solution was removed. A total of 150 μl dimethyl sulfoxide (Sigma-Aldrich; Merck KGaA) was added to each well. Subsequently, the mixture was shaken for 10 min. A microplate reader was employed to determine the optical density value at 1, 2, 3, 4 and 5 days at 490 nm.

Marker of proliferation Ki67 (Ki67) staining to detect cell proliferation. BMSCs were digested with trypsin and were incubated in a 48-well plate, on which cover slips were placed. The culture medium was aspirated out 24 h later, followed by washing in water three times. 1x10^5/ml cells were then fixed in 4% paraformaldehyde at room temperature for 20 min, followed by washing with 0.1% Triton X-100 in PBS at room temperature for 5 min on the shaking table and two PBS (0.01 mol/l) washes (5 min per wash). Subsequently, the cells were blocked by 10% normal goat serum (Abcam, Cambridge, UK) at 37˚C in an incubator for 1 h. Primary rabbit antibody against Ki67 (1:100; cat. no. ab16667; Abcam) was added, followed by incubation at 4˚C overnight. On the next day, cells were rinsed by 0.1% Triton X-100 in PBS for 5 min and 0.01 mol/l PBS twice (5 min per wash). A FITC-conjugated goat anti-rabbit secondary antibody (1:1,000; cat. no. ab6717; Abcam) was added, followed by incubation at 37˚C in an incubator for 2 h. The cells were washed with 0.01 mol/l PBS three times (5 min per wash) on a shaking table. DAPI was incubated with the cells at 37˚C in an incubator for 10 min, followed by washing with 0.01 mol/l PBS 3 times (5 min per wash). Cells were mounted in antifade mounting medium (Beyotime Institute of Biotechnology, Shanghai, China) and observed under a fluorescence inverted microscope (magnification, x400; Shanghai Dianying Optical Instrument, Co., Ltd., Shanghai, China). A total of 10 fields of view were randomly selected from each group to count the positive cells, and the positive staining rate (%)=(number of Ki67 staining positive cells/total number of cells) x100 was calculated.

Alkaline phosphatase (ALP) staining to detect osteogenesis capacity. The BMSCs of mice were cultured for 14 days and the cell density was adjusted to 1x10^5 cell/ml. The culture medium was removed and the cells were washed by PBS three times. Following trypsin digestion, cells were centrifuged at 160 x g at 4˚C for 5 min and the supernatant removed. Subsequently, 1 ml culture medium was added to suspend the cells and the suspended cells were cultured in a 6-well plate, on which sterile cover slips had been placed. The cells grew to adhere to the wall of wells fully for 6 h at 37˚C. The cover slips of each well were taken out. The revised calcium-cobalt method was adopted to stain cells (23). The cells were observed under a light microscope (magnification, x100; Shanghai Dianying Optical Instrument, Co., Ltd.) with 10 fields of view randomly selected, and the ALP staining positive cells and total cells were counted. The positive staining rate was calculated: ALP positive staining rate (%)=(number of ALP staining positive cells/total number cells) x100.

Fabrication of β-tricalcium phosphate (β-TCP) scaffolds. Cylindrical β-TCP material (Shanghai Bio-lu Biomaterials Co., Ltd., Shanghai, China) was used as composite scaffolds (24), with a porosity of 90.7±1.9%, pore diameter of 300-500 μm, diameter of 22 mm and thickness of 3 mm. On a clean table, 24 sterile packaged β-TCP scaffolds were immersed in Dulbecco's modified Eagle's medium (Gibco; Thermo Fisher Scientific, Inc.) in a 5% CO_2 incubator at 37˚C. After 48 h, β-TCP scaffolds were taken out and rinsed with Dulbecco's modified Eagle's medium containing 10% FBS five times. Both uninfected and infected BMSCs were centrifuged at 168 x g for 3 min at room temperature, followed by the addition of DMEM low-glucose medium (Gibco; Thermo Fisher Scientific, Inc.) to prepare cell suspension (5x10^6 cells/ml). The dry and sterile β-TCP scaffolds were dripped with 1 ml of the cell suspension and shaken gently to allow the suspension to fully infiltrate the pores. The scaffolds were then incubated at 37˚C in 5% CO_2 and saturated at humidity for 8 h. The solution was renewed every other day for seven days.

Mouse model establishment of repair of cranial bone defects (25). Under sterile conditions, the skin on the cranium of anesthetized mice was cut open in the midline to 5 cm. The full-thickness of the skin was separated, and the periosteum was stripped. A ring with a diameter of 22 mm was drilled into the parietal region of the mouse cranium to form a round full-thickness bone defect with a diameter of 5 mm. The bone

pieces were stripped carefully without injuring the cerebral dura mater. During this process, Hanks' balanced salt solution (Covidien, Mansfield, MA, USA) was used for rinsing and cooling. After bleeding was stopped with a gelatin sponge, corresponding prepared implants were implanted into the defect areas to fill the whole area. Subsequently, an absorbable suture was employed to suture the incision on the skin.

Micro-computed tomography (micro-CT) to detect bone regeneration. Two months following surgery, mice from all groups were euthanized. The whole cranium was separated and scanned using micro-CT. The working voltage was 55 kV, the working current was 145 mA, the depth of scanning layer was 20 μm and the scanning time was 3,400 msec. The bone regeneration conditions were analyzed and the bone volume of newly formed bones was calculated. Subsequently, the cranium specimen was separated into two parts along the midline. One part was immediately frozen in liquid nitrogen and stored in a refrigerator at -80˚C to perform RT-qPCR and western blotting. The other part of the cranium was fixed in a 10% formalin solution (Wuhan Boster Biological Technology, Ltd., Wuhan, China) at 4˚C for 24 h. The fixed sample was decalcified with 10% EDTA (pH=7.4) for 2 weeks, followed by graded dehydration and paraffin-embedding on the following day. The cranium was sliced, with a thickness of a ~6 μm, successively parallel to the long axis, from the inside out.

Histological examination of bone regeneration. Hematoxylin and eosin (H&E) staining was performed at room temperature to observe bone regeneration conditions of the newly formed bones. Slices were put into xylene for 15 min, washed with 100% anhydrous ethanol for 3 min, 90% ethanol for 3 min and 75% ethanol for 3 min, followed by gradient ethanol dewaxing to water. Hematoxylin staining was performed for 5 min, followed by washing and soaking in PBS for 5 min, eosin staining for 2 min, washing with water, gradient alcohol dehydration, xylene treatment twice for 5 min each and neutral resin blocked cover slips. Subsequently, the newly formed bone tissues were observed under an optical microscope (magnification, x400). Toluidine blue staining was employed at room temperature to observe the degradation conditions of the implanted scaffolds in the area of bone defects: Descending ethanol series followed by dewaxing and 1% toluidine blue staining for 3 min, washed with water, gradient alcohol dehydration, xylene treatment twice for 5 min each and neutral resin blocked cover slips. The staining results were observed under an optical microscope (magnification, x400).

RT-qPCR to detect mRNA expression of miR-26a, Runx2 and OC. Frozen cranium tissues from 4 mice were placed into a mortar. Following supplementation with a small amount of liquid nitrogen, the cranium tissues were ground to powder, which was transferred to Eppendorf tubes containing 1 ml TRIzol (Life Technologies; Thermo Fisher Scientific, Inc.). Shaking was performed to fully lyse the tissues. The mixture was centrifuged at 16,100 x g at 4˚C for 15 min and the supernatant was collected. Subsequently, 200 μl chloroform was added. The mixture was shaken for 15 sec to make it turn milky white and was incubated at room temperature for 5 min, followed by centrifugation at 16,100 x g at 4˚C for 15 min. The aqueous phase (400 μl) was collected. Subsequently, acid phenolics (400 μl) were extracted twice, followed by centrifugation at 16,100 x g at 4˚C for 15 min. Isopropyl alcohol (400 μl) was added, followed by inversion 4-5 times for blending and allowed to stand for 8 min at room temperature (400 μl). Centrifugation was performed at 16,100 x g at 4˚C for 10 min. The deposit was rinsed with 1 ml 75% ethanol twice and centrifuged at 6,288 x g rpm at 4˚C for 5 min. The deposit was inverted and dried for 10 min. RNase-free water (30 μl) was supplemented to dissolve the deposit. Ultra-violet analysis and formaldehyde gel electrophoresis were used to validate the high quality of the extracted RNA. RNA (1 μg) was reverse transcribed to obtain cDNA using Prime Script™ RT-PCR kit (Takara Biotechnology Co., Ltd., Dalian, China) according to the manufacturer's protocols, and the reverse transcription sample were put into the reverse transcriptome. The reverse transcription reaction conditions were 16˚C for 30 min, 42˚C for 42 min and 85˚C for 5 min. The RNA samples were reversely transcribed into cDNA (10 μl) according to the manufacturer's protocols. The obtained cDNA was diluted in 65 μl of diethyl phosphorocyanidate. The PCR mixture comprised the following elements: 5 μl of SsoFast EvaGreen Supermix (1708882; Bio-Rad Laboratories, Inc., Hercules, CA, USA), 0.5 μl of forward primer (10 μM), 0.5 μl of reverse primer (10 μM) and 4 μl of cDNA. Primers for qPCR were designed and synthesized by Invitrogen (Thermo Fisher Scientific, Inc.), with GAPDH and U6 as the internal control (Table I). The thermocycling conditions for PCR were as follows: Predenaturation at 94˚C for 5 min, followed by 40 cycles of denaturation at 94˚C for 40 sec, annealing for 40 sec at 60˚C and DNA strand extension for 1 min at 72˚C, and final extension for 10 min at 72˚C. The CFX96 qPCR machine (Bio-Rad, Inc., Hercules, CA, USA) was used. The results were analyzed by OpticonMonitor version 3 software (Bio-Rad Laboratories, Inc.). The quantification value was manually selected at the lowest point of all of the parallel rising logarithmic amplification curves, and the cycle quantification (Cq) value of

Table I. Primer sequences for reverse transcription-quantitative polymerase chain reaction.

Gene	Primer sequence
miR-26a	F: 5'-GGATCCGCAGAAACTCCAGAGA-3'
	R: 5'-TTGGAGGAAAGACGATTTCCGT-3'
U6	F:5'-ATTGGAACGATACAGAGAAGATT-3'
	R: 5'-GGAACGCTTCACGAATTTG-3'
Runx2	F: 5'-TGAGCGACGTGAGCCCGGTA-3'
	R: 5'-CGTGTGGAAGACAGCGGCGT-3'
OC	F: 5'-CCTGGCAGGTGCAAAGCCCA-3'
	R: 5'-TGCGCTTGTAGGCGTCCTGG-3'
GAPDH	F: 5'-CAAGTTCAACGGCACAGTCA-3'
	R: 5'-CCCCATTTGATGTTAGCGGG-3'

miR-26a, microRNA-26a; RUNX2, Runt-related transcription factor 2; OC, osteocalcin; GAPDH, glyceraldehyde-3-phosphate dehydrogenase; F, forward; R, reverse.

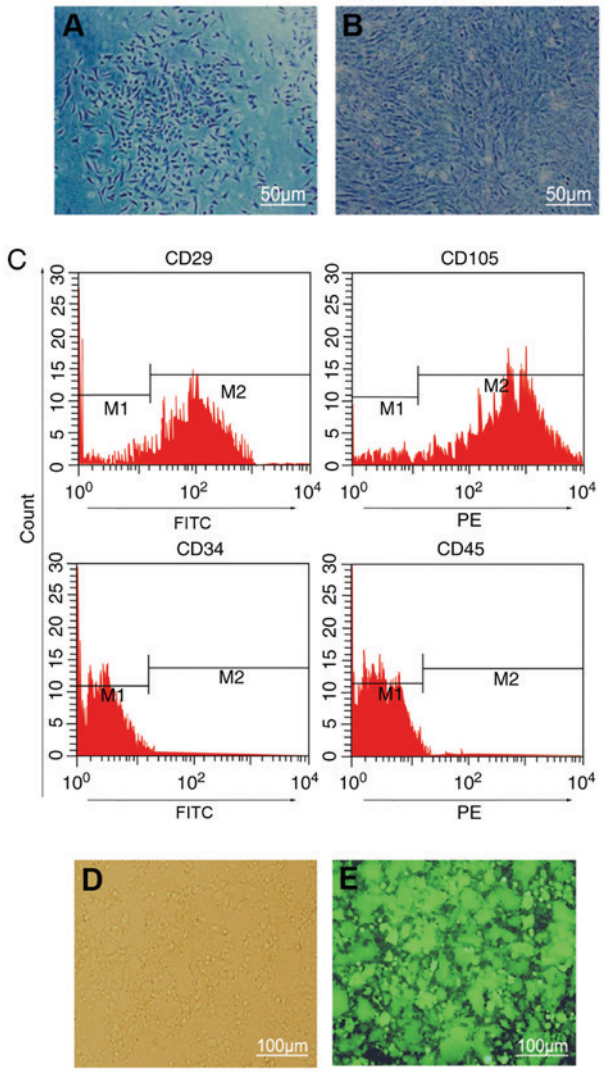

Figure 1. Cell characteristics of mouse BMSCs. Mouse BMSCs cultured for (A) 12 days and (B) 15 days. Compared with BMSCs cultured for 12 days, BMSCs cultured for 15 days demonstrated growth and increased cell numbers. (C) Expression of surface markers CD29, CD105, CD34 and CD45 on mouse BMSCs was determined by flow cytometry. CD29 and CD105 surface markers were highly expressed in isolated BMSCs, while only low expression of CD34 and CD45 was observed. (D) 293T cells prior to transfection with the lentiviral vector pLVTHM-miR-26a without GFP expression. (E) 293T cells with GFP expression following transfection with the lentiviral vector pLVTHM-miR-26a. BMSCs, bone marrow mesenchymal stem cells; miR, microRNA; GFP, green fluorescent protein.

each reaction tube was recorded. The $2^{-\Delta\Delta Cq}$ method (26) was used to compare the association of target gene expression in the experimental group and that of the blank group: $\Delta\Delta Cq=(Cq_{\text{target gene}}-Cq_{\text{control gene}})_{\text{experimental group}}-(Cq_{\text{target gene}}-Cq_{\text{control gene}})_{\text{blank group}}$.

Western blot analysis to detect protein expression of Runx2 and OC. The cranium specimens of the remaining 4 mice were taken out and washed with ice-cold PBS three times. The samples were then treated with radioimmunoprecipitation assay lysis buffer (Beyotime Institute of Biotechnology). Following thorough grinding, the samples were subjected to an ice bath for 30 min to lyse the tissues. Tissues were then centrifuged at 894 x g at 4˚C for 10 min and the supernatant collected. The protein concentration was measured by a BCA protein assay kit (Wuhan Boster Biological Technology, Ltd., Wuhan, China), according to the manufacturer's protocol. The extracted proteins were boiled with loading buffer at 95˚C for 10 min and each well was loaded with 30 μg samples. Subsequently, 10% polyacrylamide gel electrophoresis was performed to separate proteins with a voltage of 80-120 V. The separated proteins were transferred onto polyvinylidene difluoride membranes by wet transfer with a transmembrane voltage of 100 mV for 45-70 min. The membranes were blocked with 5% BSA at room temperature for 1 h. Primary antibodies against Runx2 and OC (1:1,000; cat. no. ab23981 and ab93876, respectively) and primary antibody against β-actin (1:3,000; cat. no. ab8227; both Abcam) were added at 4˚C overnight. Following washing with Tris-buffered saline with 20% Tween-20 (TBST) three times (5 min per wash), anti-rabbit secondary antibody (1:2,000; cat. no. ab205718; Abcam) was added and incubated at room temperature for 1 h. Chemiluminescence reagents (BeyoECL PLUS kit; cat. no. P0018; Beyotime Institute of Biotechnology) were added as a chromogen after the membranes were washed three times (5 min per wash). β-actin was set as the internal control. Images of the gels were captured in a Bio-Rad Gel Doc EZ Imager (Bio-Rad Laboratories, Inc.). The target protein bands were analyzed using ImageJ software (version 1.8.0; National Institutes of Health, Bethesda, MD, USA). The experiment was repeated three times and the mean value was calculated.

Statistical analysis. SPSS 21.0 software (IBM Corp., Armonk, NY, USA) was used for data analysis. Data are presented as the mean ± standard deviation. Comparisons among multiple groups were conducted by one- or two-way analysis of variance followed by Tukey's post-hoc test. $P<0.05$ was considered to indicate a statistically significant difference.

Results

Analysis of isolated BMSCs by morphology and immunophenotype. An inverted microscope was used to observe the morphological changes of mouse BMSCs. Primary cultured BMSCs had a long fusiform or oval shape that resembled fibroblasts. During subculturing, BMSCs began to adhere to the wall at approximately 3 h; to proliferate at approximately 3 days, with accumulated cell numbers, and to grow logarithmically for ~6-15 days, with increasing growth rates and a monolayer growth adherent to the wall (Fig. 1A and B).

The surface markers of separated BMSCs were detected by flow cytometry, and the results indicated that cultured BMSCs of the third generation highly expressed surface markers such as CD29 (94.2±2.1%) and CD105 (95.8±2.5%), but did not express surface markers such as CD34 (2.5±0.7%) and CD45 (1.8±0.4%; Fig. 1C). The flow cytometric detection findings were consistent with the immunophenotype of BMSCs, confirming that mouse BMSCs were successfully separated from mouse tissues.

DNA fragments of the full-length hairpin pre-miR-26a and its flanking sequence were amplified by PCR and a specific band of ~194 bp was identified by electrophoresis. Verified by dual-enzyme (*Mlu I* and *Cla I*) digestion, recombinant plasmids produced fragments of approximately 11 kb and 194 bp, consistent with the predicted results. In addition, the sequencing

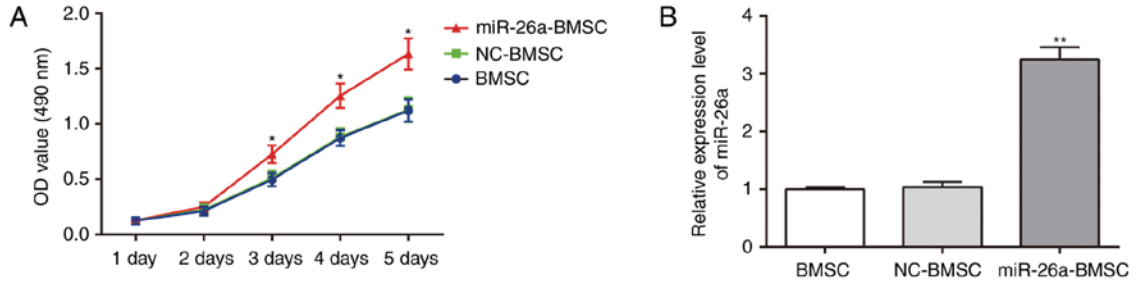

Figure 2. Comparison of the cell growth and expression levels of miR-26a in BMSCs prior to and following lentiviral infection. Uninfected BMSCs and BMSCs transfected with NC or miR-26a vectors were investigated. (A) Cell viability of each group. Two-way analysis of variance followed by Tukey's post-hoc test was employed for statistical comparisons. (B) miR-26a expression in BMSCs of each group. The experiments were repeated three times and mean values were calculated. One-way analysis of variance followed by Tukey's post-hoc test was employed for statistical comparisons. *P<0.05 and **P<0.01 vs. BMSC group. The BMSC group refers to uninfected BMSCs. miR, microRNA; BMSCs, bone marrow mesenchymal stem cells; NC, negative control; OD, optical density.

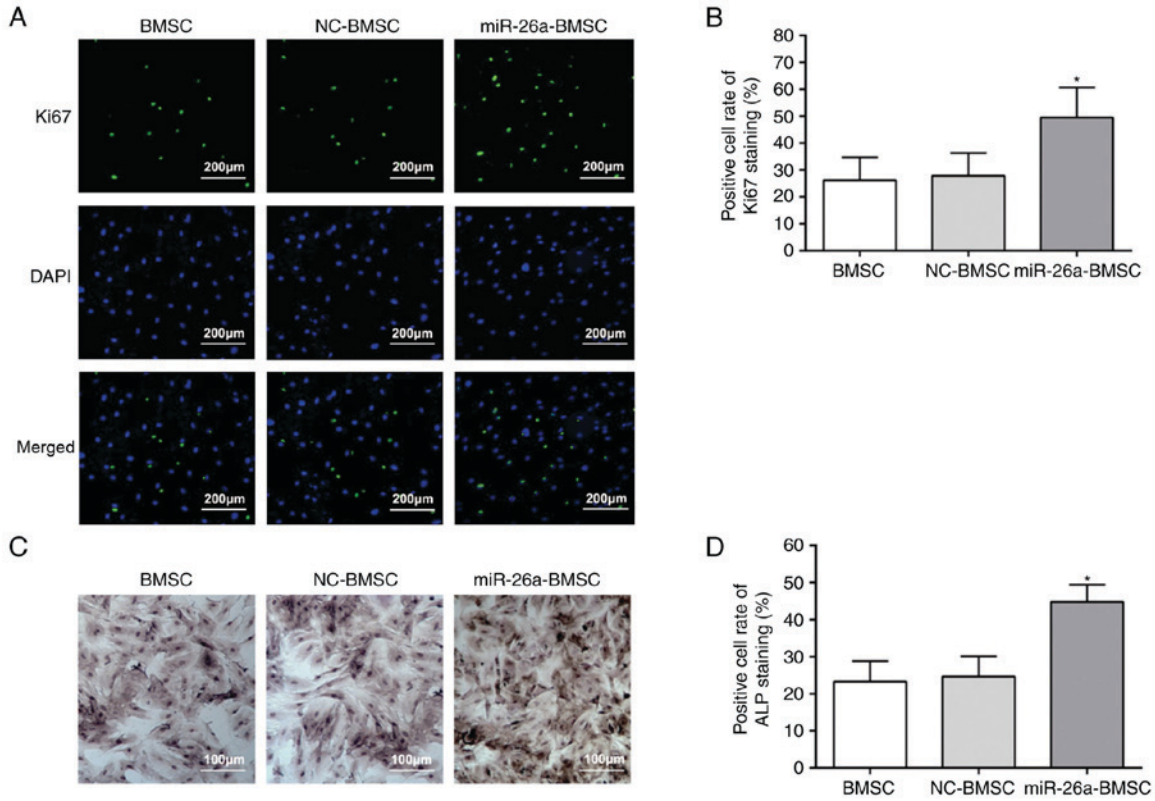

Figure 3. Comparison of the cell proliferation and osteogenic capacity of different groups. Uninfected BMSCs and BMSCs transfected with NC or miR-26a vectors were investigated. (A) Ki67 staining observed by fluorescence inverted microscope (magnification, x400). (B) Positive cell rate of Ki67 staining. (C) ALP staining observed by confocal microscopy. (D) Positive cell rate of ALP staining. The experiments were repeated three times and the mean values were calculated. One-way analysis of variance followed by Tukey's post-hoc test was employed for statistical comparisons. *P<0.05 vs. BMSC group. The BMSC group refers to uninfected BMSCs. BMSCs, bone marrow mesenchymal stem cells; NC, negative control; miR, microRNA; Ki67, marker of proliferation Ki67; ALP, alkaline phosphatase.

results were the same as the precursor miRNA sequences in the miRBase database (data not shown). Following a graded dilution, the packaged lentiviral particles were transfected into 293T cells and the expression of green fluorescent protein (GFP) was observed under a light microscope and a fluorescence inverted microscope (Fig. 1D and E). The number of GFP-positive 293T cells in each well was quantified, and the determined lentiviral titer was $5x10^5$ TU/ml.

Cell viability and expression levels of miR-26a in BMSCs prior to and following lentiviral infection. An MTT assay was conducted to identify the viability of BMSCs in different groups (Fig. 2A). No significant differences were observed in BMSC viability between uninfected BMSCs and BMSCs infected with the pLVTHM empty vector (P>0.05). However, marked increases in the viability of BMSCs infected with pLVTHM-miR-26a were observed from day 3 compared with uninfected BMSCs (P<0.05). The cells of all groups grew continuously and the growth of these cells was not inhibited by cytotoxicity. To validate successful lentiviral infection, RT-qPCR was conducted to detect miR-26a expression prior to and following lentiviral infection. Compared with uninfected

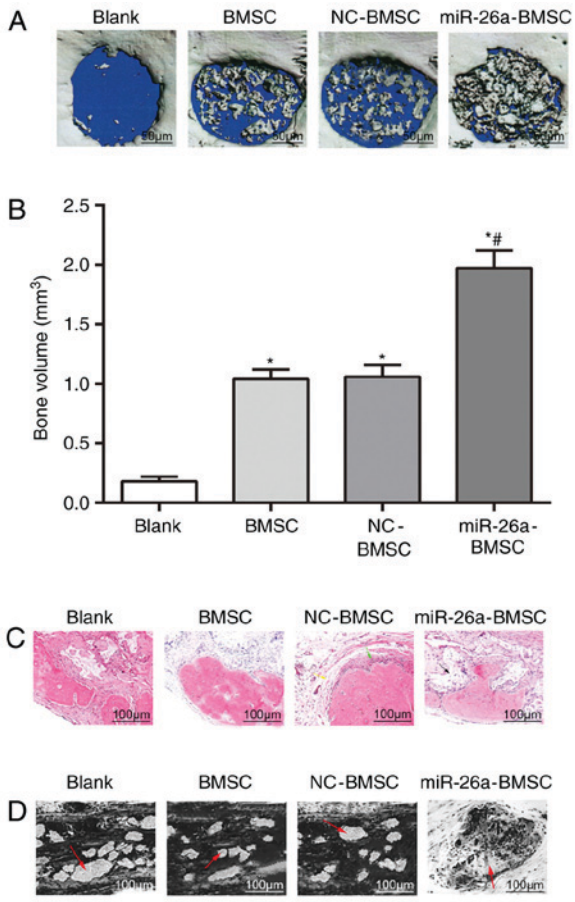

Figure 4. Comparison of the bone regeneration of mice from different groups. (A) Comparison of the bone regeneration conditions in the defect areas of mice from different groups detected by micro-computed tomography. (B) Quantitative analysis of the bone volume of newly formed bones in the defect areas of mice from different groups. (C) Hematoxylin and eosin staining for detecting the regeneration conditions of bone tissues in the defect area. The yellow arrow indicates scar tissue, the green arrow indicates the inflammatory cells and the black arrow indicates the new bone tissue. (D) Toluidine blue staining for detecting the degradation conditions of the scaffolds. The arrows indicate scaffolds that were not degraded. Two-way analysis of variance followed by Tukey's post-hoc test was employed for statistical comparisons. *P<0.05 vs. blank group; #P<0.05 vs. BMSC group. The BMSC group refers to uninfected BMSCs. A total of 32 mice were examined and every experiment was repeated three times, and mean values were calculated. BMSCs, bone marrow mesenchymal stem cells; NC, negative control; miR, microRNA.

BMSCs, BMSCs infected with pLVTHM-miR-26a exhibited significantly increased miR-26a expression (P<0.01), and BMSCs infected with empty vector pLVTHM were not significantly different compared with uninfected BMSCs (P>0.05), indicating that BMSCs were successfully infected with the lentiviral vector pLVTHM-miR-26a (Fig. 2B).

Effect of miR-26a on cell proliferation and osteogenic capacity of BMSCs. Ki67 is a marker for cell proliferation, and a higher positive rate of Ki67 reflects more active cell proliferation (27). The results of Ki67 and ALP staining are demonstrated in Fig. 3. The BMSCs of all groups had Ki67-positive cells (Fig. 3A) and the positive rate of the miR-26a-BMSC group was markedly higher compared with the uninfected BMSC and BMSC-NC groups (Fig. 3B). No difference was identified between the uninfected BMSC and BMSC-NC groups (Fig. 3B). Furthermore, the results of ALP staining (Fig. 3C) indicated that, following culture for 14 days, all groups exhibited varying positive reactions, and brown or black granules and blocks appeared in the cytoplasm. Compared with the uninfected BMSC group, the miR-26a-BMSC group demonstrated an increased ALP positive rate (P<0.05), while the uninfected BMSC group and the NC-BMSC group were not significantly different (Fig. 3D). These findings indicated that miR-26a may facilitate the osteogenic capacity of BMSCs.

Bone regeneration in the defect areas of mice from different groups. The conditions of newly formed bones in the defect area were observed using micro-CT. The results (Fig. 4A) indicated that mice in the blank group implanted with β-TCP scaffolds alone in the defect area did not demonstrate newly formed bones. Mice in the BMSC group, implanted with β-TCP scaffolds co-cultured with uninfected BMSCs in the defect area, and mice in the NC-BMSC group, implanted with β-TCP scaffolds co-cultured with NC-BMSCs in the defect area, exhibited a few scattered newly formed bones. Mice in the miR-26a-BMSC group, implanted with β-TCP scaffolds co-cultured with miR-26a-BMSCs in the defect area, presented a marked increase in newly formed bones compared with the BMSC and NC-BMSC groups, which almost filled the whole defect area (Fig. 4A).

Bone volume of newly formed bones in the defect areas of mice from different groups. Quantitative analysis was performed on the bone volume of newly formed bones in the defect areas (Fig. 4B). Compared with the blank group, the bone volume of newly formed bones in the BMSC and BMSC-NC groups was significantly increased (P<0.05), indicating that BMSCs promoted bone regeneration in bone defect repair. Furthermore, compared with the BMSC group, the bone volume of newly formed bones in the miR-26a-BMSC group was further increased (P<0.05), indicating that lentivirus-mediated miR-26a overexpression in BMSCs enhanced bone regeneration in bone defect repair in mice.

Bone regeneration and degradation of implanted scaffolds in the defect areas of mice from different groups. To further verify the effects of miR-26a on bone regeneration in the repair of cranial bone defects, H&E staining was conducted to observe the bone regeneration conditions in the defect areas. In the defect areas of mice from the 4 groups, mice in the miR-26a-BMSC group demonstrated regeneration of bone tissues. Even staining of newly formed bone tissues was observed. Spindle-shaped osteoblasts were observed in the margin of newly formed bones. Erythrocytes were observed inside and surrounding newly formed bones and scattered in newly formed blood vessels. Mice in the BMSC and BMSC-NC groups demonstrated minimal regeneration of bone tissues in addition to some bone cells, and mice in the blank group did not demonstrate regeneration of bone tissues (Fig. 4C).

Toluidine blue staining was performed to observe the degradation conditions of implanted scaffolds in the bone defect areas of the cranium (Fig. 4D). In the blank group, scaffolds that were not degraded and enveloped by fibrosis were observed in the defect area. In the BMSC and BMSC-NC

groups, the scaffolds were gradually degraded and scaffolds that were not degraded were scattered. In the miR-26a-BMSC group, the majority of scaffolds were degraded and replaced by newly formed bone tissues.

Expression levels of osteogenesis-associated cytokines in the defect areas of mice from different groups. RT-qPCR and western blot analysis were performed to detect the mRNA and protein expression of the osteogenesis-associated cytokines Runx2 and OC (Fig. 5). Compared with the blank group, the mRNA and protein expression of Runx2 and OC in the BMSC and BMSC-NC groups were elevated ($P<0.05$). The mRNA (Fig. 5A) and protein (Fig. 5B and C) expression of Runx2 and OC in the miR-26a-BMSC group was also increased compared with the blank group ($P<0.05$), and also significantly higher compared with the BMSC group ($P<0.05$), indicating that lentiviral-mediated miR-26a overexpression in BMSCs may enhance bone regeneration in bone defect repair.

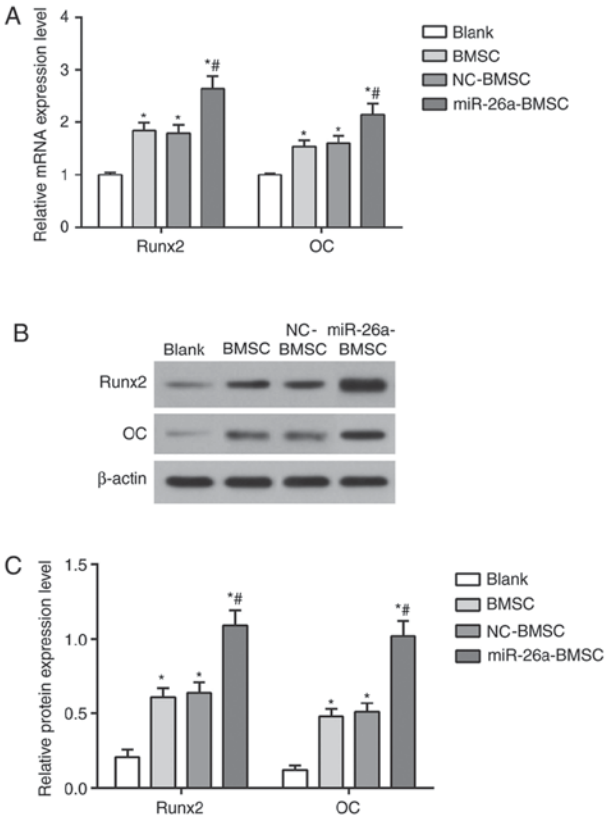

Figure 5. Comparison of mRNA and protein expression of osteogenic-associated cytokines in the defect areas of mice from different groups by RT-qPCR and western blot analysis. (A) mRNA levels of the osteogenic-associated cytokines Runx2 and OC in the defect areas of the BMSC and NC groups were significantly higher compared with the blank group, and expression in the miR-26a-BMSC group was markedly higher compared with the BMSC and NC groups, as measured by RT-qPCR. (B) Representative western blot bands for Runx2 and OC protein expression in mice in the different treatment groups. (C) Densitometric analysis was performed to quantify the expression of protein and the results were consistent with those for mRNA expression. The experiments were repeated three times and the mean values were calculated. Two-way analysis of variance followed by Tukey's post-hoc test was employed for statistical comparisons. *$P<0.05$ vs. blank group; #$P<0.05$ vs. BMSC group. The BMSC group refers to uninfected BMSCs. RT-qPCR, reverse transcription-quantitative polymerase chain reaction; Runx2, runt-related transcription factor 2; OC, osteocalcin; BMSCs, bone marrow mesenchymal stem cells; NC, negative control; miR, microRNA.

Discussion

Repair of bone defects presents a serious clinical challenge as it is difficult to restore bone function and regenerate bone loss (28). To address this issue, the present study proposed miR-26a as a potential therapeutic target, and lentivirus-mediated miR-26a overexpression was used to genetically modify BMSCs in the repair of cranial bone defects in mice. Delivery of BMSCs modified by miR-26a to β-TCP scaffold-filled defect areas markedly enhanced bone regeneration and novel bone formation, and also intensified the BMSC proliferation capacity.

Initially, the present study successfully constructed the lentiviral vector pLVTHM-miR-26a, which upregulated the expression levels of miR-26a in BMSCs from mice. BMSCs overexpressing miR-26a markedly increased bone regeneration and the volume of newly formed bones, and also promoted BMSC proliferation. Concerning the association between miRNAs and bone diseases, Seeliger *et al* (29) highlighted that five miRNAs, which included miR-21, miR-23a, miR-24, miR-25 and miR-100, were elevated in the bone tissue and serum of patients suffering from osteoporosis. Despite the documented effects of miRNAs on osteoclastogenesis, osteoblastogenesis and osteogenesis, their clinical value remains poorly defined (30,31). The present study went further by combining miR-26a with BMSCs and β-TCP scaffolds. The results of *in vitro* and *in vivo* experiments in one study have demonstrated that transfection of miR-26a significantly accelerated the osteogenic differentiation of adipose-derived stem cells *in vitro* and enhanced new bone formation following miR-26a transfection *in vivo* (32). Furthermore, the repair response to critical calvarial bone defects was demonstrated to be strengthened through positive modulation of miR-26a in angiogenic-osteogenic coupling (33). The underlying mechanism by which miR-26a positively mediates angiogenic-osteogenic coupling may be due to the fact that its high expression in newly formed bones increases vascular endothelial growth factor (VEGF) secretion. Bone, which is a highly vascularized tissue, relies on coordinated angiogenic-osteogenic coupling to regenerate (34). miR-26a has been reported to be implicated in VEGF-mediated angiogenesis through the regulation of endothelial nitric oxide synthase activity, which is modulated by its effect on NUS1 dehydrodolichyl diphosphate synthase subunit (NgBR) expression by directly targeting the NgBR 3'-UTR (35). miRNAs are crucial regulators of the differentiation of BMSCs. For example, upregulated miR-16 expression has been reported to promote BMSC arrest in the G1 phase and enhance the differentiation of BMSCs of a cardiac niche towards the myogenic phenotype (10,11).

In the present study, β-TCP scaffolds loaded with miR-26a-modified and GFP-labeled BMSCs were implanted into defect areas in mouse models of cranial bone defects. Subsequently, the regeneration and volume of newly formed bones were demonstrated to be markedly increased compared with the blank, uninfected BMSC and BMSC-NC groups. Similar findings were identified in a previous study, which demonstrated that β-TCP scaffolds seeded with osteogenically induced BMSCs significantly repaired critically sized

mandibular defects in canine models as osteoclast-like cells may originate in precursors of mononuclear myeloid cells and lead to angiogenesis or migration from the microenvironment to scaffolds (36). Multipotent and undifferentiated BMSCs enable cells to transform into differentiated types, producing similar phenotypic expression to that of the resident cells of a particular tissue, such as bone (37). Mesenchymal stem cells (MSCs) and MSC-derived endothelial cells are reported to complement one another and facilitate the vascularization of biomaterials and the degree of bone regeneration (38). Furthermore, Dupont *et al* (39) stated that porous scaffolds augmented with stem cells accelerated the repair response to large segmental bone defects. Notably, the microenvironment and surrounding tissues facilitate MSC differentiation by secreting growth factors, nutrients and extracellular matrices, and MSCs are reprogrammed during gene expression (40).

To further confirm the initial findings of the present study, the mRNA and protein expression of osteogenesis-associated cytokines, including Runx2 and OC, in mice treated with the various types of BMSCs and β-TCP scaffolds were detected using RT-qPCR and western blot analysis. The results demonstrated that mice implanted with β-TCP scaffolds co-cultured with miR-26a-BMSCs in the defect area demonstrated significantly elevated mRNA and protein expression of Runx2 and OC compared with the blank group, and the levels were even higher compared with the uninfected BMSC and BMSC-NC groups. Su *et al* (41) reported that overexpression of miR-26a increased ALP activity and Runx2 mRNA expression levels in BMSCs. Another study by Luzi *et al* (19) also demonstrated that upregulation of miR-26a expression elevated the expression of OC in bone diseases. It is widely accepted that the expression levels of Runx2 and OC may be detected to evaluate bone regeneration, and osteogenesis influences BMSCs by enhancing the formation of blood vessels, producing osteogenic cues and delivering osteoblastic progenitors at the same time (7).

In conclusion, the present study provided promising evidence that modified BMSCs by lentivirus-mediated miR-26a may facilitate the repair of cranial bone defects in mouse models and that β-TCP scaffolds seeded with BMSCs exhibit satisfactory regeneration and formation of new bones. However, a limitation for the present study is that quantitative examination in terms of degradation rate was not performed, and only qualitative degradation conditions of each group were observed based on the toluidine blue staining. As the degradation of β-TCP matched the regeneration of newly formed bone tissues, the degradation conditions could be demonstrated by conditions of newly formed bone tissues. Despite this limitation, the present study may provide a potential therapeutic target for the treatment of bone defects. Further investigations should focus on transferring the theoretical hypothesis to clinical practice with quantitative examination of the degradation rate.

Acknowledgements

Not applicable.

Funding

No funding was received.

Availability of data and materials

The analyzed data sets generated during the study are available from the corresponding author on reasonable request.

Authors' contributions

ZL and BY designed the study. ZL, BY and HC wrote the manuscript. HC and YH researched relevant references and established the methodology. YW and ZZ acquired the data. MW and ZH analyzed and interpreted the data.

Ethics approval and consent to participate

The present study was approved by the Experimental Animal Ethics Committee of the People's Hospital of Dongsheng.

Patient consent for publication

Not applicable.

Competing interests

The authors declare that they have no competing interests.

References

1. Kolambkar YM, Boerckel JD, Dupont KM, Bajin M, Huebsch N, Mooney DJ, Hutmacher DW and Guldberg RE: Spatiotemporal delivery of bone morphogenetic protein enhances functional repair of segmental bone defects. Bone 49: 485-492, 2011.
2. Calori GM, Mazza E, Colombo M and Ripamonti C: The use of bone-graft substitutes in large bone defects: Any specific needs? Injury 42 (Suppl 2): S56-S63, 2011.
3. Lv J, Xiu P, Tan J, Jia Z, Cai H and Liu Z: Enhanced angiogenesis and osteogenesis in critical bone defects by the controlled release of BMP-2 and VEGF: Implantation of electron beam melting-fabricated porous Ti6Al4V scaffolds incorporating growth factor-doped fibrin glue. Biomed Mater 10: 035013, 2015.
4. Kusumbe AP, Ramasamy SK and Adams RH: Coupling of angiogenesis and osteogenesis by a specific vessel subtype in bone. Nature 507: 323-328, 2014.
5. Kolambkar YM, Dupont KM, Boerckel JD, Huebsch N, Mooney DJ, Hutmacher DW and Guldberg RE: An alginate-based hybrid system for growth factor delivery in the functional repair of large bone defects. Biomaterials 32: 65-74, 2011.
6. Li J, Hong J, Zheng Q, Guo X, Lan S, Cui F, Pan H, Zou Z and Chen C: Repair of rat cranial bone defects with nHAC/PLLA and BMP-2-related peptide or rhBMP-2. J Orthop Res 29: 1745-1752, 2011.
7. Zou D, Zhang Z, Ye D, Tang A, Deng L, Han W, Zhao J, Wang S, Zhang W, Zhu C, *et al*: Repair of critical-sized rat calvarial defects using genetically engineered bone marrow-derived mesenchymal stem cells overexpressing hypoxia-inducible factor-1α. Stem Cells 29: 1380-1390, 2011.
8. Zhang Y, Wang F, Chen J, Ning Z and Yang L: Bone marrow-derived mesenchymal stem cells versus bone marrow nucleated cells in the treatment of chondral defects. Int Orthop 36: 1079-1086, 2012.
9. Lin CY, Chang YH, Lin KJ, Yen TC, Tai CL, Chen CY, Lo WH, Hsiao IT and Hu YC: The healing of critical-sized femoral segmental bone defects in rabbits using baculovirus-engineered mesenchymal stem cells. Biomaterials 31: 3222-3230, 2010.
10. Liu JL, Jiang L, Lin QX, Deng CY, Mai LP, Zhu JN, Li XH, Yu XY, Lin SG and Shan ZX: MicroRNA 16 enhances differentiation of human bone marrow mesenchymal stem cells in a cardiac niche toward myogenic phenotypes in vitro. Life Sci 90: 1020-1026, 2012.
11. Chen S, Yang L, Jie Q, Lin YS, Meng GL, Fan JZ, Zhang JK, Fan J, Luo ZJ and Liu J: MicroRNA125b suppresses the proliferation and osteogenic differentiation of human bone marrowderived mesenchymal stem cells. Mol Med Rep 9: 1820-1826, 2014.

12. Xu JF, Yang GH, Pan XH, Zhang SJ, Zhao C, Qiu BS, Gu HF, Hong JF, Cao L, Chen Y, *et al*: Altered microRNA expression profile in exosomes during osteogenic differentiation of human bone marrow-derived mesenchymal stem cells. PLoS One 9: e114627, 2014.
13. Zhang J, Han C and Wu T: MicroRNA-26a promotes cholangiocarcinoma growth by activating β-catenin. Gastroenterology 143: 246-256 e248, 2012.
14. Mohamed JS, Lopez MA and Boriek AM: Mechanical stretch up-regulates microRNA-26a and induces human airway smooth muscle hypertrophy by suppressing glycogen synthase kinase-3β. J Biol Chem 285: 29336-29347, 2010.
15. Yang X, Liang L, Zhang XF, Jia HL, Qin Y, Zhu XC, Gao XM, Qiao P, Zheng Y, Sheng YY, *et al*: MicroRNA-26a suppresses tumor growth and metastasis of human hepatocellular carcinoma by targeting interleukin-6-Stat3 pathway. Hepatology 58: 158-170, 2013.
16. Leeper NJ, Raiesdana A, Kojima Y, Chun HJ, Azuma J, Maegdefessel L, Kundu RK, Quertermous T, Tsao PS and Spin JM: MicroRNA-26a is a novel regulator of vascular smooth muscle cell function. J Cell Physiol 226: 1035-1043, 2011.
17. Bahi A, Chandrasekar V and Dreyer JL: Selective lentiviral-mediated suppression of microRNA124a in the hippocampus evokes antidepressants-like effects in rats. Psychoneuroendocrinology 46: 78-87, 2014.
18. Sun BS, Dong QZ, Ye QH, Sun HJ, Jia HL, Zhu XQ, Liu DY, Chen J, Xue Q, Zhou HJ, *et al*: Lentiviral-mediated miRNA against osteopontin suppresses tumor growth and metastasis of human hepatocellular carcinoma. Hepatology 48: 1834-1842, 2008.
19. Luzi E, Marini F, Tognarini I, Galli G, Falchetti A and Brandi ML: The regulatory network menin-microRNA 26a as a possible target for RNA-based therapy of bone diseases. Nucleic Acid Ther 22: 103-108, 2012.
20. Luzi E, Marini F, Sala SC, Tognarini I, Galli G and Brandi ML: Osteogenic differentiation of human adipose tissue-derived stem cells is modulated by the miR-26a targeting of the SMAD1 transcription factor. J Bone Miner Res 23: 287-295, 2008.
21. Ye JH, Xu YJ, Gao J, Yan SG, Zhao J, Tu Q, Zhang J, Duan XJ, Sommer CA, Mostoslavsky G, *et al*: Critical-size calvarial bone defects healing in a mouse model with silk scaffolds and SATB2-modified iPSCs. Biomaterials 32: 5065-5076, 2011.
22. Williams JR: The declaration of Helsinki and public health. Bull World Health Organ 86: 650-652, 2008.
23. Mikheev AG: 2 modifications of the calcium-cobalt method for cytochemical determination of alkaline phosphatase in leukocytes of the blood and bone marrow. Lab Delo 12: 711-713, 1969 (In Russian).
24. Li J, Jin L, Wang M, Zhu S and Xu S: Repair of rat cranial bone defect by using bone morphogenetic protein-2-related peptide combined with microspheres composed of polylactic acid/polyglycolic acid copolymer and chitosan. Biomed Mater 10: 045004, 2015.
25. Xu L, Lv K, Zhang W, Zhang X, Jiang X and Zhang F: The healing of critical-size calvarial bone defects in rat with rhPDGF-BB, BMSCs, and β-TCP scaffolds. J Mater Sci Mater Med 23: 1073-1084, 2012.
26. Livak KJ and Schmittgen TD: Analysis of relative gene expression data using real-time quantitative PCR and the 2(-Delta Delta C(T)) method. Methods 25: 402-408, 2001.
27. Li TJ, Browne RM and Matthews JB: Epithelial cell proliferation in odontogenic keratocysts: A comparative immunocytochemical study of Ki67 in simple, recurrent and basal cell naevus syndrome (BCNS)-associated lesions. J Oral Pathol Med 24: 221-226, 1995.
28. Giannoudis PV, Faour O, Goff T, Kanakaris N and Dimitriou R: Masquelet technique for the treatment of bone defects: Tips-tricks and future directions. Injury 42: 591-598, 2011.
29. Seeliger C, Karpinski K, Haug AT, Vester H, Schmitt A, Bauer JS and van Griensven M: Five freely circulating miRNAs and bone tissue miRNAs are associated with osteoporotic fractures. J Bone Miner Res 29: 1718-1728, 2014.
30. van Wijnen AJ, van de Peppel J, van Leeuwen JP, Lian JB, Stein GS, Westendorf JJ, Oursler MJ, Im HJ, Taipaleenmäki H, Hesse E, *et al*: MicroRNA functions in osteogenesis and dysfunctions in osteoporosis. Curr Osteoporosis Rep 11: 72-82, 2013.
31. Li KC, Chang YH, Yeh CL and Hu YC: Healing of osteoporotic bone defects by baculovirus-engineered bone marrow-derived MSCs expressing MicroRNA sponges. Biomaterials 74: 155-166, 2016.
32. Wang Z, Zhang D, Hu Z, Cheng J, Zhuo C, Fang X and Xing Y: MicroRNA-26a-modified adipose-derived stem cells incorporated with a porous hydroxyapatite scaffold improve the repair of bone defects. Mol Med Rep 12: 3345-3350, 2015.
33. Paquet J, Moya A, Bensidhoum M and Petite H: Engineered cell-free scaffold with two-stage delivery of miRNA-26a for bone repair. Ann Transl Med 4: 204, 2016.
34. Li Y, Fan L, Liu S, Liu W, Zhang H, Zhou T, Wu D, Yang P, Shen L, Chen J and Jin Y: The promotion of bone regeneration through positive regulation of angiogenic-osteogenic coupling using microRNA-26a. Biomaterials 34: 5048-5058, 2013.
35. Jo HN, Kang H, Lee A, Choi J, Chang W, Lee MS and Kim J: Endothelial miR-26a regulates VEGF-Nogo-B receptor-mediated angiogenesis. BMB Rep 50: 384-389, 2017.
36. Yuan J, Zhang WJ, Liu G, Wei M, Qi ZL, Liu W, Cui L and Cao YL: Repair of canine mandibular bone defects with bone marrow stromal cells and coral. Tissue Eng Part A 16: 1385-1394, 2010.
37. Tian H, Bharadwaj S, Liu Y, Ma PX, Atala A and Zhang Y: Differentiation of human bone marrow mesenchymal stem cells into bladder cells: Potential for urological tissue engineering. Tissue Eng Part A 16: 1769-1779, 2010.
38. Zhou J, Lin H, Fang T, Li X, Dai W, Uemura T and Dong J: The repair of large segmental bone defects in the rabbit with vascularized tissue engineered bone. Biomaterials 31: 1171-1179, 2010.
39. Dupont KM, Sharma K, Stevens HY, Boerckel JD, Garcia AJ and Guldberg RE: Human stem cell delivery for treatment of large segmental bone defects. Proc Natl Acad Sci USA 107: 3305-3310, 2010.
40. Hasegawa N, Kawaguchi H, Hirachi A, Takeda K, Mizuno N, Nishimura M, Koike C, Tsuji K, Iba H, Kato Y and Kurihara H: Behavior of transplanted bone marrow-derived mesenchymal stem cells in periodontal defects. J Periodontol 77: 1003-1007, 2006.
41. Su X, Liao L, Shuai Y, Jing H, Liu S, Zhou H, Liu Y and Jin Y: MiR-26a functions oppositely in osteogenic differentiation of BMSCs and ADSCs depending on distinct activation and roles of Wnt and BMP signaling pathway. Cell Death Dis 6: e1851, 2015.